Direct Growth of Bilayer Graphene on SiO_2 Substrates by Carbon Diffusion through Nickel

Zhiwei Peng,[†,∥] Zheng Yan,[†,∥] Zhengzong Sun,[†] and James M. Tour[†,‡,§,*]

[†]Department of Chemistry, [‡]Department of Mechanical Engineering and Materials Science, and the [§]Richard E. Smalley Institute for Nanoscale Science and Technology, Rice University, 6100 Main Street, Houston, Texas 77005, United States. [∥]These authors contributed equally to this work.

ABSTRACT Here we report a transfer-free method of synthesizing bilayer graphene directly on SiO_2 substrates by carbon diffusion through a layer of nickel. The 400 nm nickel layer was deposited on the top of SiO_2 substrates and used as the catalyst. Spin-coated polymer films such as poly(methyl methacrylate), high-impact polystyrene or acrylonitrile–butadiene–styrene, or gas-phase methane were used as carbon sources. During the annealing process at 1000 °C, the carbon sources on the top of the nickel decomposed and diffused into the nickel layer. When cooled to room temperature, bilayer graphene was formed between the nickel layer and the SiO_2 substrates. The nickel films were removed by etchants, and bilayer graphene was then directly obtained on SiO_2, eliminating any transfer process. The bilayer nature of the obtained graphene films on SiO_2 substrates was verified by Raman spectroscopy and transmission electron microscopy. The Raman spectroscopy mapping over a 100 × 100 μm^2 area indicated that the obtained graphene is high-quality and bilayer coverage is approximately 70%.

KEYWORDS: bilayer graphene · synthesis · solid carbon source · chemical vapor deposition · Raman spectroscopy · TEM

Graphene, as a single layer of sp^2-bonded carbon atoms packed into a two-dimensional honeycomb crystal lattice, has attracted much interest since its first isolation in 2004.[1] Due to its superb properties such as high carrier mobility, chemical stability, optical transparency, and low density, graphene has been seen as an excellent material for electronic, optical, and sensor devices.[2−4] However, the semimetal and zero band-gap electronic structure of pristine monolayer graphene limit its further electronic and optical applications.[5] Thus, much effort has been focused on the study of bilayer graphene, because AB-stacked (Bernal) bilayer graphene would have a tunable band gap, while twisted bilayer graphene would show angle-dependent electronic properties.[6−13] Both chemical vapor deposition (CVD) and solid carbon sources can be used to fabricate graphene films with controlled thickness on metal substrates.[14−24] However, in these methods, the obtained graphene films need to be separated from metal substrates and transferred to insulating substrates for further electronic processing. Recently, our group developed a new pathway to grow large-scale bilayer graphene directly on insulating substrates without a further transfer process.[25] In that method, the solid carbon source was deposited between nickel layers and insulating substrates and was then directly transformed into bilayer graphene at 1000 °C. In the experiments, we found the carbon between the nickel films and insulating substrates could diffuse into the nickel films and form graphene on the top and bottom surface of the nickel upon cooling. Inspired by these experiments, we now place the carbon sources on the top of the nickel and find that bilayer graphene also forms between the insulating substrates and nickel layers due to carbon diffusion.

Here, we demonstrate a facile synthesis of bilayer graphene directly on SiO_2 substrates by the diffusion and precipitation of carbon in nickel layers. The carbon sources come from either solid polymer films of poly(methyl methacrylate) (PMMA), high impact polystyrene (HIPS), or acrylonitrile–butadiene–styrene (ABS), or gas flow of methane on the top side of nickel layers. When the samples were annealed under Ar/H_2 flow and at 1000 °C, the carbon sources decomposed and the carbon dissolved and diffused into the nickel layer and deposited on both sides of the nickel to form graphene upon cooling. After etching away the nickel, bilayer graphene was obtained directly on the SiO_2 substrates.

RESULTS AND DISCUSSION

Figure 1 illustrates the procedure for the growth of bilayer graphene directly on the SiO_2 substrate. The SiO_2 substrate was cleaned with oxygen-plasma and Piranha solution (4:1 sulfuric acid/hydrogen peroxide), and then a 400 nm thick nickel film was

* Address correspondence to tour@rice.edu.

Received for review August 1, 2011 and accepted September 3, 2011.

Published online September 03, 2011
10.1021/nn202923y

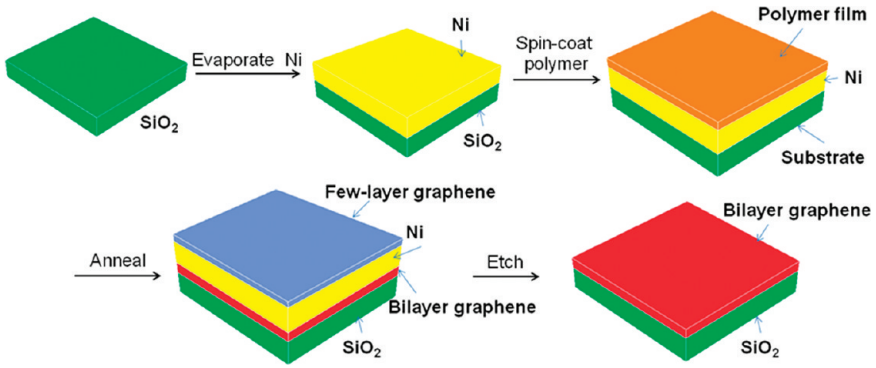

Figure 1. Schematics of the growth of bilayer graphene from a solid carbon source. A 400 nm nickel film was thermally evaporated onto SiO_2 substrate, followed by the spin-coating of polymers on the nickel. After annealing samples at 1000 °C under a reductive Ar/H_2 pressure for ~10 min and then etching away the nickel, bilayer graphene is obtained directly on SiO_2. The polymer film formation can be replaced by exposure to methane during the annealing step.

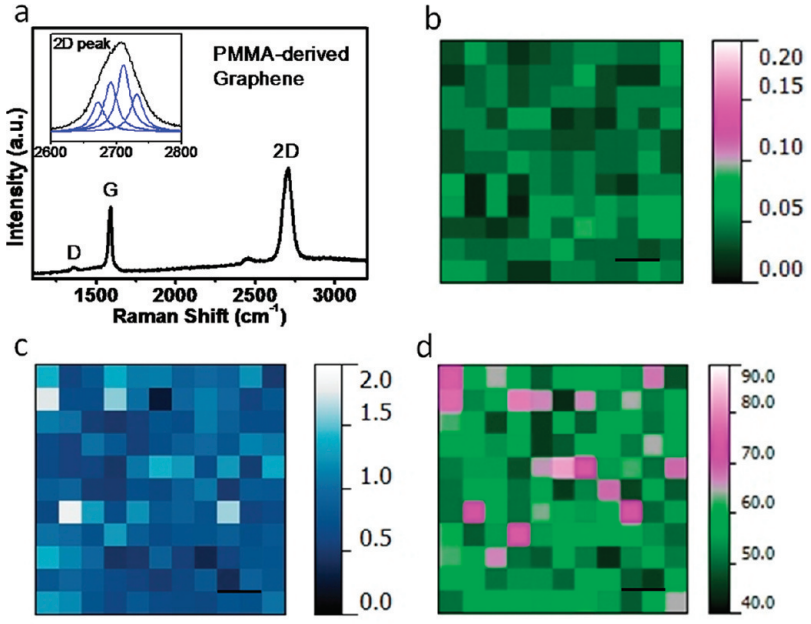

Figure 2. Raman spectra of PMMA-derived bilayer graphene. (a) Typical Raman spectrum of PMMA-derived bilayer graphene. The inset shows that the 2D peak can be deconvoluted into four components: $2D_{1B}$, $2D_{1A}$, $2D_{2A}$, and $2D_{2B}$ from the left to the right. (b) D/G peak ratio mapping of the PMMA-derived bilayer graphene film over a 100 × 100 μm^2 area. (c) G/2D peak ratio mapping of the PMMA-derived bilayer graphene film over a 100 × 100 μm^2 area. (d) fwhm Raman mapping of the PMMA-derived bilayer graphene film over a 100 × 100 μm^2 area. The scale bar in (b), (c), and (d) is 20 μm.

thermally evaporated onto the top of the SiO_2 substrate used as the metal catalyst. Either solid polymers (PMMA, HIPS, or ABS) or gas-phase methane was used as a carbon source for the transfer-free growth of bilayer graphene. For the solid carbon source, the polymers were spin-coated onto the top of the nickel film, followed by annealing samples at 1000 °C for ~10 min with a reductive gas flow (H_2/Ar) under low-pressure conditions (~7 Torr). For the gas carbon source, methane was used during the annealing process under ambient pressure. Detailed growth procedures are summarized in the Experimental Section. During the annealing process, the carbon sources decomposed, and dissolved and diffused in the nickel film. Upon fast cooling, carbon precipitated from the nickel film and formed graphene on both sides of the nickel film. After dissolving away the nickel film together with graphene on its top using Marble's reagent, bilayer graphene was obtained directly on the SiO_2 substrate, eliminating any transfer process.

With PMMA used as the solid carbon source for the transfer-free growth of bilayer graphene on SiO_2, Raman spectroscopy was used to analyze the number of layers and the quality of the graphene. Figure 2a is the typical Raman spectrum of the PMMA-derived bilayer graphene on SiO_2, showing that the G peak at ~1580 cm^{-1} and the 2D peak at ~2700 cm^{-1} are comparable in intensity, and the full-width at half-height maximum (fwhm) of the 2D peak is about 50 cm^{-1}. Furthermore, the 2D peak (the inset in Figure 2a) is asymmetric and can be deconvoluted into four small peaks, $2D_{1B}$, $2D_{1A}$, $2D_{2A}$, and $2D_{2B}$, which correspond to four permissible photon

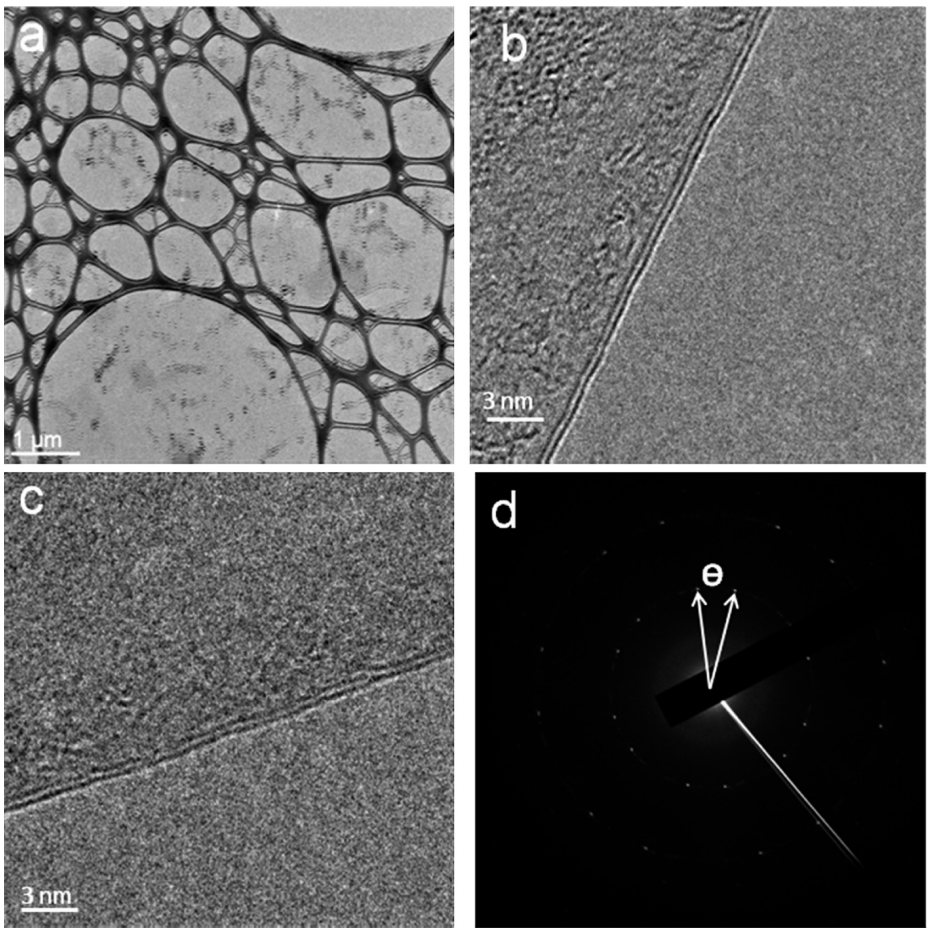

Figure 3. TEM analysis of PMMA-derived bilayer graphene. (a) Low-resolution TEM image showing bilayer graphene films over a large area on a TEM grid. (b and c) HRTEM images of bilayer graphene edges that show two carbon layers. (d) Hexagonal SAED pattern of the bilayer graphene that shows a rotation angle of ~12° between the two layers.

transitions in graphene.[26−29] The 2D peak position, fwhm, and shape, together with the G to 2D peak ratio, all indicate that PMMA-derived graphene on SiO_2 is bilayered.[20,21,24−30] The small D peak at ~1350 cm^{-1} in Figure 2a suggests that PMMA-derived bilayer graphene has few defects or symmetry-broken sites. The high quality of PMMA-derived bilayer graphene over large areas was demonstrated by the Raman mapping of the D to G peak intensity ratio. Figure 2b shows that the D to G peak ratio over around ~99% area is below 0.1, suggesting the high quality of the obtained graphene film. A four-probe measurement of the graphene film shows a sheet resistance of ~2000 Ω/sq, which further confirms the high quality of the PMMA-derived graphene film.[22] The uniformity and the coverage of PMMA-derived bilayer graphene were determined by Raman mapping of the G to 2D peak intensity ratio (Figure 2c) and 2D peak fwhm (Figure 2d) over a 100 × 100 μm^2 area. Considering that many factors could affect the Raman spectra of graphene,[15,21−23] we set a range of the G to 2D peak ratio from 0.7 to 1.3 and the fwhm of the 2D peak from 45 to 60 cm^{-1} to estimate the bilayer coverage.[15,22,23] Those that have a G to 2D peak ratio lower than 0.7 and fwhm of 2D peak lower than 45 cm^{-1} are considered to be monolayer graphene, and the samples that have a G to 2D peak ratio higher than 1.3 and fwhm of the 2D peak higher than 60 cm^{-1} are considered few-layer graphene. According to this criterion, the bilayer graphene coverage was ~70%. Monolayer and few-layer graphene can also be found in ~20% and ~10% of the area, respectively, and their typical Raman spectra are summarized in Figure S1.

PMMA-derived bilayer graphene was further characterized by TEM. The graphene film was removed from the SiO_2 substrate using buffered oxide etch and then transferred onto TEM grids for further characterization. The suspended graphene films on the TEM grids are continuous over a large area, as shown in low-resolution TEM (Figure 3a). Randomly imaged graphene edges (Figure 3b and c) show two carbon layers, verifying the bilayer nature of the graphene film.[24] The randomly selected area electron diffraction (SAED) pattern clearly shows two typical hexagonal crystalline structures of graphene with a small angle θ. In Figure 3d specifically, θ is about 12°, but in other areas θ could be from 0° to 30°. If we reduced the spot size of the SAED analysis, two sets of hexagonal diffraction patterns were still found. We also did FFT calculation in

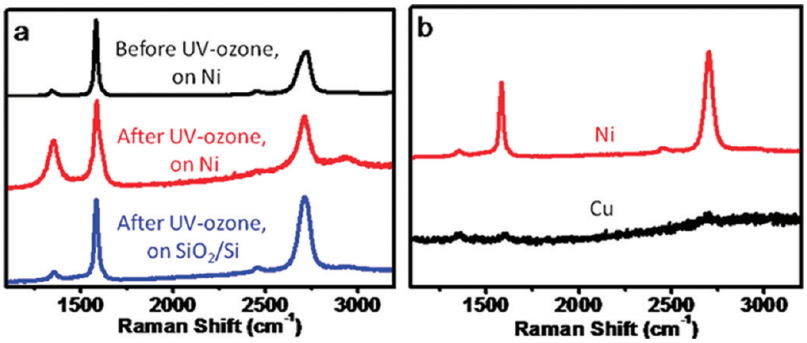

Figure 4. Raman spectroscopic analysis of graphene from different growth conditions. (a) Raman spectra of graphene on the top of the nickel layer before and after UV-ozone exposure, and graphene on the substrate after UV-ozone exposure and nickel removal. (b) Raman spectra of PMMA-derived graphene by different metal catalysts.

an area as small as 20 × 20 nm^2, as shown in Figure S2. Two sets of hexagonal diffraction patterns remained, indicating that the obtained graphene layers are non-Bernal (non-AB) stacked. Although some areas appear to be Bernal (AB) stacked by only one 6-fold symmetric pattern, most of the bilayer graphene (~95%) is non-Bernal. We cannot determine whether the angle results from transfer to the TEM grid or during the growth process. There is a possibility that the SAED patterns in Figure 3d and FFT patterns in Figure S2 come from two very small single domains (<20 × 20 nm^2) of Bernal bilayer graphene. But such highly polycrystalline graphene film should have a larger D peak in the Raman spectrum, which has not been observed in our case.

A carbon diffusion mechanism is proposed for the growth mechanism of bilayer graphene on SiO_2 substrates. During the annealing process at 1000 °C, the PMMA decomposed, dissolved, and diffused into the whole nickel film due to high solubility of carbon in nickel. When the sample is removed from the hot zone of the furnace and rapidly cools, carbon precipitates from both sides of the nickel layer to form graphene films. In most cases, few-layer graphene was obtained on the top of nickel (see the black curve in Figure 4a). However, after etching the nickel films, bilayer graphene was obtained directly on SiO_2, as the constrained environment between the nickel film and the SiO_2 substrate apparently benefited the growth of bilayer graphene.

A control experiment was conducted and is shown in Figure 4a, demonstrating that the graphene layer on the SiO_2 is not from the top side of the nickel. The black curve in Figure 4a shows that the graphene on the top side of the nickel has a small D peak with $I_D/I_G < 0.1$. After being treated by UV-ozone for 15 min, the D peak increases, with $I_D/I_G \approx 0.8$, indicating the graphene film on the top of nickel was badly damaged. After etching the nickel film using Marble's reagent, bilayer graphene with a small D peak was still obtained on SiO_2. From this control experiment, it is evident that the bilayer graphene on the SiO_2 is indeed formed underneath the nickel layer and is not from the top of the nickel layer. As a comparison, copper was also used as the catalyst for the transfer-free growth of graphene. Here a 400 nm copper film was deposited on the SiO_2 substrate, PMMA was used as the carbon source, and other conditions are similar to that of nickel. However, after etching the copper film using Marble's reagent, almost no carbon was obtained on the SiO_2 substrate (the black curve in Figure 4b). From this result it is apparent that carbon has too low a solubility in copper and it is difficult for carbon to diffuse below the copper film.[31] Recently, Su *et al.* used a thinner copper layer to grow graphene between the metal layer and substrate.[32] In their case, methane was used as the continuous carbon supply, and it is proposed that the carbon can diffuse through the copper layer at the grain boundaries.

The above-proposed growth mechanism of bilayer graphene was further supported by the following experiments. The amount of PMMA on the top of the nickel was adjusted by changing the spin-coating speed and time, and its effect on the graphene growth was determined. Figure 5a demonstrates that all four spin-coating speeds led to the growth of bilayer graphene on SiO_2 substrates, suggesting that the constrained environment between nickel films and SiO_2 substrates plays a major role in the growth of bilayer graphene. However, if none of the carbon source was put on top of the nickel, nothing was obtained on the SiO_2 under similar growth conditions (see Figure S3 in the SI). Meanwhile, the effects of nickel film thickness on bilayer graphene growth were also investigated. Figure 5b shows that nickel film thickness has a limited effect on the bilayer graphene growth since all three nickel film thicknesses, 400, 250, and 170 nm, led to the formation of bilayer graphene on SiO_2. However, when the thickness of the nickel film was decreased below 170 nm, most of the nickel evaporated during the annealing process at 1000 °C and results in the growth of discontinuous graphene with a large D peak.

Different annealing temperatures were also used for the growth of PMMA-derived bilayer graphene. Figure 5c demonstrates that the lower limit of annealing temperature for high-quality graphene growth is ~900 °C; when the annealing temperature was lowered to 800 °C, the obtained bilayer graphene had a

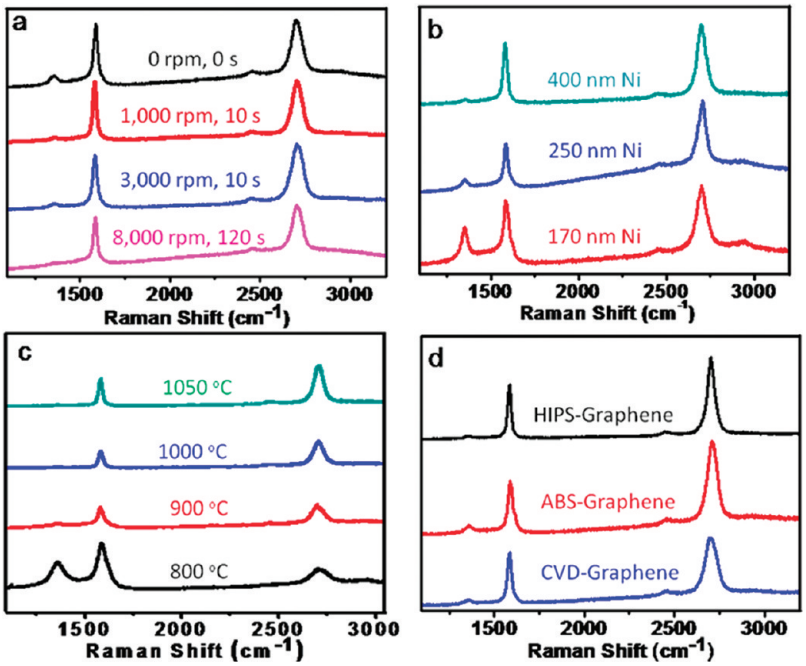

Figure 5. Raman spectra of bilayer graphene from different carbon sources and UV-ozone experiments. (a) Raman spectra of bilayer graphene films of different PMMA thicknesses by adjusting spin-coating speeds. (b) Raman spectra of PMMA-derived graphene with different thicknesses of nickel layers. (c) Raman spectra of PMMA-derived graphene grown at different temperatures. (d) Raman spectra of HIPS-, ABS-, and CVD-derived bilayer graphene.

large D peak in the Raman spectrum, with $I_D/I_G \approx 0.7$. This was also consistent with previous experiments, where a lower growth temperature would cause a larger D peak.[33] Other polymers including HIPS and ABS were also deposited on the top of the nickel film and used as solid carbon sources for the transfer-free growth of graphene. The Raman spectra in Figure 5d indicate that both HIPS and ABS lead to the formation of bilayer graphene on SiO_2 substrates. The Raman mapping of the G/2D peak ratio, D/G peak ratio, and fwhm of HIPS-derived graphene in Figure S4 indicate that the quality of HIPS-derived bilayer graphene is almost as high as PMMA-derived graphene. For ABS-derived graphene, a larger D peak is observed with $I_D/I_G \approx 0.2$. This is because ABS contains nitrogen elements in its chemical structure and results in the formation of nitrogen-doped graphene, which is further supported by X-ray photoemission spectroscopy (XPS) characterization (Figure S5). The N1s peak at ~400 eV can be deconvoluted into two peaks located at 399.6 and 401.2 eV, corresponding to pyridinic N and quaternary N in graphene, respectively. A gas-phase carbon source, methane, was also used for the transfer-free growth of graphene on SiO_2 substrates (Figure S6). The blue curve in Figure 5d indicates that methane-derived graphene is also bilayered. This is further proven by TEM images of CVD-derived graphene in Figure S7. The effects of methane flow rates on graphene growth were investigated and are shown in Figure S8. The result shows that when the flow rate of methane is larger than 60 sccm, the D peak of the obtained graphene is minimized, and in all cases bilayer graphene is still the major adduct. This also indicates that the key factor for the growth of bilayer graphene is the constrained environments between nickel films and SiO_2 substrates instead of the amount of carbon source.

CONCLUSION

In summary, we have developed a facile synthesis method for large-scale and high-quality bilayer graphene directly on SiO_2 substrates by carbon diffusion through nickel layers, eliminating any transfer process. Moreover, it does not require the deposition of metal on top of a precise thickness of polymer film as in our previous protocol.[25] This scalable method should be compatibile with graphene-based electronic device fabrication needs. This growth method of high-quality bilayer graphene would further facilitate the future research and applications of graphene.

EXPERIMENTAL SECTION

Synthesis of Graphene Film. The bilayer graphene films were synthesized by carbon diffusion into the nickel layer and precipitation below the bottom of the nickel layer. Prior to evaporating the nickel layer, the 500 nm thick SiO_2/Si^{++} substrates underwent a surface cleaning by oxygen-plasma etching for 10 min, followed by immersion in Piranha solution (4:1 sulfuric acid/hydrogen peroxide) at 95 °C for 30 min, sonication

(Fisher Scientific FS110H) in DI water for at least 60 min, thoroughly rinsing with DI water, and drying under a nitrogen flow, and further drying in a vacuum oven (~100 Torr) at 80 °C for 30 min. Then, an Edwards Auto 306 thermal evaporator was used to deposit the nickel layer on the top of the substrates. Nickel powder (low carbon, Puratronic, 99.999%, C < 100 ppm) was used as the nickel source and was loaded into an Al_2O_3 boat. The substrates were fixed on the ceiling of the chamber. The nickel was deposited at the rate of ~0.3 nm/s when the chamber pressure was $\sim 1 \times 10^{-6}$ Torr. For graphene growth from solid carbon sources, the polymer film was formed on substrates by spin-coating 200 μL of polymer solution at 3000 rpm for 40 s. The PMMA solution was 950 PMMA A4 from MicroChem Corp. and was used without further treatment. HIPS solution was made by dissolving HIPS (0.4 g, Poly One, 478W 69, lot # VF1801RZ78) in anhydrous toluene (11.1 mL). ABS solution was made by dissolving ABS (0.4 g, Poly One, PD1090 60, lot # VE0601QD32) in THF (10.80 mL). The substrates were put into a standard 1 in. quartz tube furnace for 7 to 20 min at 1000 °C while feeding H_2 (50−600 sccm) and Ar (500 sccm) at a total pressure of ~7 Torr. A copper enclosure formed by bending 25 μm thick copper foil (Alfa Aesar, 99.98%) was used to cover the substrates to trap trace O_2 and carbon in the system. For CVD growth, the synthesis was conducted under ambient pressure conditions with H_2 (50−600 sccm) and methane (20−100 sccm). The samples were fast-cooled to room temperature by quickly removing them from the hot zone of the furnace using a magnetic rod device. After the growth, Marble's reagent ($CuSO_4$/HCl/H_2O in a wt/vol/vol ratio of 10 g:50 mL:50 mL) was used as the etchant to remove the nickel layer by placing the sample into the solution for 1 min, followed by washing in a mixture of DI water and ethanol (10 mL:10 mL) for 30 s and drying with a nitrogen flow.

Characterizations. Raman spectra and mapping images of graphene films were measured with a Renishaw RE02 Raman microscope using 514 nm laser excitation at room temperature. A 2100F field emission gun transmission electron microscope was used to take the high-resolution TEM images of graphene samples transferred onto a lacey carbon (Ted Pella) or a C-flat TEM grid (Protochips). XPS was performed on a PHI Quantera SXM scanning X-ray microprobe with 100 μm beam size and 45° takeoff angle.

Acknowledgment. We thank the ONR MURI (No. 00006766, N00014-09-1-1066), the AFRL through United Technology Corporation (FA8650-05-D-5807), the AFOSR (FA9550-09-1-0581), and M-I SWACO for funding.

Supporting Information Available: Raman spectra, Raman mapping, XPS spectra, fabrication schematic, and TEM are available free of charge *via* the Internet at http://pubs.acs.org.

Note Added after ASAP Publication: This paper was published on September 14, 2011 without all of the required corrections. Figure 4 was corrected and various other typographical changes were made. The corrected version was reposted on September 23, 2011.

REFERENCES AND NOTES

1. Novoselov, K. S.; Geim, A. K.; Morozov, S. V.; Jiang, D.; Zhang, Y.; Dubonos, S. V.; Grigorieva, I. V.; Firsov, A. A. Electric Field Effect in Atomically Thin Carbon Films. *Science* **2004**, *306*, 666–669.
2. Geim, A. K.; Novoselov, K. S. The Rise of Graphene. *Nat. Mater.* **2007**, *6*, 183–191.
3. Novoselov, K. S.; Geim, A. K.; Morozov, S. V.; Jiang, D.; Katsnelson, M. I.; Grigorieva, I. V.; Dubonos, S. V.; Firsov, A. A. Two-Dimensional Gas of Massless Dirac Fermions in Graphene. *Nature* **2005**, *438*, 197–200.
4. Zhang, Y. B.; Tan, Y. W.; Stormer, H. L.; Kim, P. Experimental Observation of the Quantum Hall Effect and Berry's Phase in Graphene. *Nature* **2005**, *438*, 201–204.
5. Castro Neto, A. H.; Guinea, F.; Peres, N. M. R.; Novoselov, K. S.; Geim, A. K. The Electronic Properties of Graphene. *Rev. Mod. Phys.* **2009**, *81*, 109–162.
6. Zhang, Y.; Tang, T.; Girit, C.; Hao, Z.; Martin, M. C.; Zettl, A.; Crommie, M. F.; Shen, Y. R.; Wang, F. Direct Observation of a Widely Tunable Bandgap in Bilayer Graphene. *Nature* **2009**, *459*, 820–823.
7. McCann, E. Asymmetry Gap in the Electronic Band Structure of Bilayer Graphene. *Phys. Rev. B* **2006**, *74*, 161403.
8. Oostinga, J. B.; Heersche, H. B.; Liu, X.; Morpurgo, A. F.; Vandersypen, L. M. K. Gate-Induced Insulating State in Bilayer Graphene Devices. *Nat. Mater.* **2008**, *7*, 151–157.
9. Castro, E. V.; Novoselov, K. S.; Morozov, S. V.; Peres, N. M. R.; Lopes dos Santos, J. M. B.; Nilsson, J.; Guinea, F.; Geim, A. K.; Castro Neto, A. H. Biased Bilayer Graphene: Semiconductor with a Gap Tunable by the Electric Field Effect. *Phys. Rev. Lett.* **2007**, *99*, 216802.
10. Novoselov, K. S.; McCann, E.; Morozov, S. V.; Fal'ko, V. I.; Katsnelson, M. I.; Zeitler, U.; Jiang, D.; Schedin, F.; Geim, A. K. Unconventional Quantum Hall Effect and Berry's Phase of 2π in Bilayer Graphene. *Nat. Phys.* **2006**, *2*, 177–180.
11. Ohta, T.; Bostwick, A.; Seyller, T.; Horn, K.; Rotenberg, E. Controlling the Electronic Structure of Bilayer Graphene. *Science* **2006**, *313*, 951–954.
12. Mak, K. F.; Lui, C. H.; Shan, J.; Heinz, T. F. Obsservation of an Electric-Field-Induced Band Gap in Bilayer Graphene by Infrared Spectroscopy. *Phys. Rev. Lett.* **2009**, *102*, 256405.
13. Luican, A.; Li, G.; Reina, A.; Kong, J.; Nair, R. R.; Novoselov, K. S.; Geim, A. K.; Andrei, E. Y. Single-Layer Behavior and Its Breakdown in Twisted Graphene Layers. *Phys. Rev. Lett.* **2011**, *106*, 126802.
14. Reina, A.; Jia, X.; Ho, J.; Nezich, D.; Son, H.; Bulovic, V.; Dresselhaus, M. S.; Kong, J. Large Area, Few-Layer Graphene Films on Arbitrary Substrates by Chemical Vapor Deposition. *Nano Lett.* **2009**, *9*, 30–35.
15. Li, X.; Cai, W.; An, J.; Kin, S.; Nah, J.; Yang, D.; Piner, R.; Celamakanni, A.; Jung, I.; Tutuc, E.; *et al.* Large-Area Synthesis of High-Quality and Uniform Graphene Films on Copper Foils. *Science* **2009**, *324*, 1312–1314.
16. Gao, L.; Guest, J. R.; Guisinger, N. P. Epitaxial Graphene on Cu(111). *Nano Lett.* **2010**, *10*, 3512–3516.
17. Ago, H.; Ito, Y.; Mizuta, N.; Yoshida, K.; Hu, B.; Orofeo, C. M.; Tsuji, M.; Ikeda, K.; Mizuno, S. Epitaxial Chemical Vapor Deposition Growth of Single-Layer Graphene over Cobalt Film Crystallized on Sapphire. *ACS Nano* **2010**, *4*), 7407–7414.
18. Li, X.; Magnuson, C. W.; Venugopal, A.; Tromp, R. M.; Hannon, J. B.; Vogel, E. M.; Colombo, L.; Ruoff, R. S. Large-Area Graphene Single Crystals Grown by Low-Pressure Chemical Vapor Deposition of Methane on Copper. *J. Am. Chem. Soc.* **2011**, *133*), 2816–2819.
19. Reddy, K. M.; Gledhill, A. D.; Chen, C.; Drexler, J. M.; Padture, N. P. High Quality, Transferrable Graphene Grown on Single Crystal Cu(111) Thin Films on Basal-Plane Sapphire. *Appl. Phys. Lett.* **2011**, *98*, 113117.
20. Lee, S.; Lee, K.; Zhong, Z. Wafer Scale Homogeneous Bilayer Graphene Films by Chemical Vapor Deposition. *Nano Lett.* **2010**, *10*, 4702–4707.
21. Yan, K.; Peng, H.; Zhou, Y.; Li, H.; Liu, Z. Formation of Bilayer Bernal Graphene: Layer-by-Layer Epitaxy via Chemical Vapor Deposition. *Nano Lett.* **2011**, *11*, 1106–1110.
22. Sun, Z.; Yan, Z.; Yao, J.; Beitler, E.; Zhu, Y.; Tour, J. M. Growth of Graphene from Solid Carbon Sources. *Nature* **2010**, *468*, 549–552.
23. Chen, S.; Cai, W.; Piner, R. D.; Suk, J. W.; Wu, Y.; Ren, Y.; Kang, J.; Ruoff, R. S. Synthesis and Characterization of Large-Area Graphene and Graphite Films on Commercial Cu-Ni Alloy Foils. *Nano Lett.* **2011**, Article ASAP, DOI: 10.1021/nl201699j.
24. Warner, J. H.; Rummel, M. H.; Gemming, T.; Buchner, B.; Briggs, G. A. D. Direct Imaging of Rotational Stacking Faults in Few Layer Graphene. *Nano Lett.* **2009**, *9*, 102–106.
25. Yan, Z.; Peng, Z.; Sun, Z.; Yao, J.; Liu, Z.; Ajayan, P. M.; Tour, J. M. *Growth of Bilayer Graphene on Insulating Substrates*. In press, DOI: 10.1021/nn202829y/.
26. Ferrari, A. C.; Meyer, J. C.; Scardaci, V.; Casiraghi, C.; Lazzeri, M.; Mauri, F.; Piscanec, S.; Jiang, D.; Novoselov, K. S.; Roth, S.; *et al.* Raman Spectrum of Graphene and Graphene Layers. *Phys. Rev. Lett.* **2006**, *97*, 187401–187404.

27. Luo, Z.; Yu, T.; Shang, J.; Wang, Y.; Lim, S.; Liu, L.; Gurzadyan, G. G.; Shen, Z.; Lin, J. Large-Scale Synthesis of Bi-layer Graphene in Strongly Coupled Stacking Order. *Adv. Funct. Mater.* **2011**, *21*, 911–917.
28. Malard, L. M.; Pimenta, M. A.; Dresselhaus, G.; Dresselhaus, M. S. Raman Spectroscopy in Graphene. *Phys. Rep.* **2009**, *473*, 51–87.
29. Malard, L. M.; Nilsson, J.; Elias, D. C.; Brant, J. C.; Plentz, F.; Alves, E. S.; Castro Neto, A. H.; Pimenta, M. A. Probing the Electronic Structure of Bilayer Graphene by Raman Scattering. *Phys. Rev. B* **2007**, *76*, 201401.
30. Hao, Y.; Wang, Y.; Wang, L.; Ni, Z.; Wang, Z.; Wang, R.; Koo, C. K.; Shen, Z.; Thong, J. T. L. Probing Layer Number and Stacking Order of Few-layer Graphene by Raman Spectroscopy. *Small* **2010**, *6*, 195–200.
31. Li, X.; Cai, W.; Colombo, L.; Ruoff, R. S. Evolution of Graphene Growth on Ni and Cu by Carbon Isotope Labeling. *Nano Lett.* **2009**, *9*, 4268–4272.
32. Su, C.; Lu, A.; Wu, C.; Li, Y.; Liu, K.; Zhang, W.; Lin, S.; Juang, Z.; Zhong, Y.; Chen, F.; Li, L. Direct Formation of Wafer Scale Graphene Thin Layers on Insulating Substrates by Chemical Vapor Deposition. *Nano Lett.* **2011**, Article ASAP, DOI: 10.1021/nl201362n.
33. Lee, C. S.; Baraton, L.; He, Z.; Maurice, J.; Chaigneau, M.; Pribat, D.; Cojocaru, C. S. Dual Graphene Films Growth Process Based on Plasma-Assisted Chemical Vapor Deposition. *Proc. SPIE* **2010**, *7761*, 77610P.